ELSEVIER

Available online at www.sciencedirect.com

SCIENCE DIRECT®

International Journal of Solids and Structures 42 (2005) 5161–5180

INTERNATIONAL JOURNAL OF SOLIDS and STRUCTURES

www.elsevier.com/locate/ijsolstr

Three-dimensional limit analysis of rigid blocks assemblages. Part II: Load-path following solution procedure and validation

A. Orduña *, P.B. Lourenço

Department of Civil Engineering, University of Minho, Azurém, 4800-058 Guimarães, Portugal

Received 7 July 2004; received in revised form 8 February 2005
Available online 17 March 2005

Abstract

A novel solution procedure for the non-associated limit analysis of rigid blocks assemblages is proposed. This proposal produces better solutions than previously proposed procedures and it is also able to provide an insight into the structural behaviour prior to failure. The limit analysis model proposed in Part I of this paper and the solution procedure are validated through illustrative examples in three-dimensional masonry piers and walls. The use of limit analysis for three-dimensional problems incorporating non-associated flow rules and a coupled yield surface is novel in the literature.

Keywords: Limit analysis; Non-associated flow rule; Rigid block; Non-linear optimisation

1. Introduction

In the first part of this paper (Orduña and Lourenço, 2005), a complete limit analysis formulation for rigid block assemblages was presented. In this formulation, it was accepted that the rigid blocks interact through quadrilateral interfaces without tensile strength and cohesion, that the non-associated Coulomb criterion governs the shearing failure, and that the compressive stresses are limited. In the development of this model, the plastic torsion on frictional interfaces was studied, and a piecewise linear yield function for rectangular interfaces was proposed together with a model for the hinging yield mode.

* Corresponding author. Present address: Faculty of Civil Engineering, University of Colima, km 9, Colima-Coquimatlán way 28400, Mexico. Tel./fax: +52 312 316 1167.
E-mail address: aord@ucol.mx (A. Orduña).

0020-7683/$ - see front matter
doi:10.1016/j.ijsolstr.2005.02.011

The standard material model (with associated flow rules) introduces important theoretical simplifications to limit analysis. The most significant result, perhaps, is the uniqueness of the ultimate load factor, defined as the ratio between the variable loads causing the collapse and their nominal values. Besides, non-standard materials were studied since the early limit analysis development stages; see for instance Palmer, 1966. More recent investigations include those of Corigliano and Maier (1995), Boulbibane and Weichert (1997) and De Saxcé and Bousshine (1998). A constant in all these investigations is the lack of unique solutions for limit analysis problems in the presence of non-associated flow rules.

The present research state in this topic can be very briefly summarised as follows. Together with the yield surface, there exist the G-surface constituted by the inner envelope of the hyperplanes perpendicular to the directions of the plastic flow vectors at each point of the yield surface; see Fig. 1. The G-surface has different names and slightly different definitions depending on the authors, however its more important feature is being completely within the yield surface. It is well known that all the points outside the yield surface are unsafe. Also, it can be demonstrated that all the points inside the G-surface are strictly safe, provided they satisfy the equilibrium requirements too. Nevertheless, nothing can be said, theoretically, about the safety of the points between both surfaces. Observe that for associated flow rules, the G-surface is identical to the yield surface and the set of indefinite safety solutions is empty.

In the particular case of friction with zero dilatancy, as is the case of concern of this paper, the G-surface is reduced to the solutions without shear forces at the interfaces. It is evident that solutions under this condition would conduct almost always to zero load factors. This result is useless in practice.

Using the concept of bipotential, De Saxcé and Bousshine (1998) recover the normality of the flow rule in an implicit sense for frictional materials. Those authors find that the lower and upper bound theorems are coupled and confirm that the limit load factor is not unique.

Baggio and Trovalusci (1998) proposed to minimise the load factor in a rigid blocks limit analysis formulation, as a way to obtain the safest solution. The formulation of the problem obtained in this way is known in the mathematical programming literature as a mathematical problem with equilibrium constraints (MPEC). There are no routines explicitly written to solve this problem type. In fact Baggio and Trovalusci (1998) proposed to solve it as a standard non-linear programming problem (NLP). Nevertheless, those authors faced serious difficulties in the solution phase. Ferris and Tin-Loi (2001) proposed another

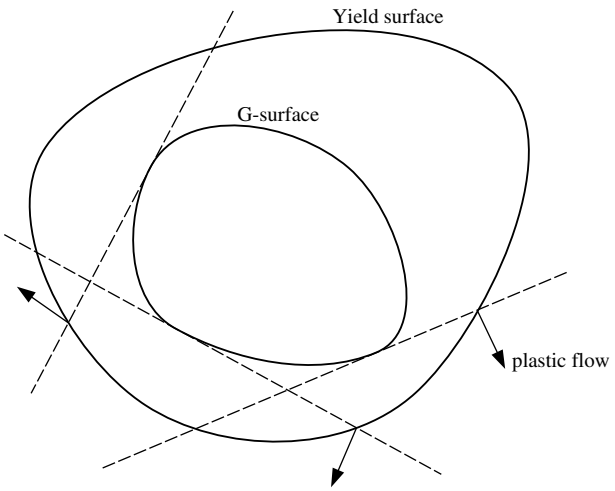

Fig. 1. Yield and G-surfaces.

solution strategy in order to minimise the load factor taking advantage of routines explicitly written for solving mixed complementarity problems (MCP), which is a problem type akin to the MPEC. The main disadvantage of the approach consisting on minimising the load factor is that the resulting ultimate load factor can severely underestimate its true value.

In this paper, a novel solution procedure is proposed for the non-associated limit analysis of rigid blocks assemblages. This procedure follows, in an approximate manner, the loading history on the structure. The procedure is useful in providing a good understanding of the structural behaviour before and at failure. And, more important, the procedure provides better solutions than minimising the load factor. Finally, both the limit analysis model and the solution procedure are validated through three illustrative examples. It is noted that the solution of three-dimensional limit analysis problems involving non-associated flow and coupled failure surfaces seems to be novel in the literature.

2. The limit analysis problem

Eqs. (1)–(6) are the conditions that a limit analysis solution with non-associated flow rule must fulfil. Eq. (1) combines the compatibility and flow rule conditions. Here, $\vec{N}_0$ is a matrix, which columns contain the flow directions corresponding to each yield mode; the vector $\delta\vec{\lambda}$ contains the flow multipliers for the yield modes; $\vec{C}$ is the compatibility matrix and the vector $\delta\vec{u}$ contains the displacement rates for all the blocks in the model. Eq. (2) is a scaling condition for the displacement rates that ensures the existence of non-zero but finite values. Here, $\vec{F}_{\mathrm{v}}$ is the vector of variable loads applied on the centroid of each block. Eq. (3) is the equilibrium condition. Here, $\vec{F}_{\mathrm{c}}$ is the constant loads vector; α is the load factor, measuring the amount of variable load applied on the structure, and $\vec{Q}$ is the vector of generalised stresses at the interfaces. Eq. (4) guarantees that the yield functions, $\vec{\varphi}$, are not violated. Eq. (5) ensures that the plastic flow multipliers are non-negative, which means that flow implies energy dissipation. Finally, Eq. (6) guarantees that plastic flow cannot occur unless the stresses have reached the yield surface. A more detailed description of the limit analysis mathematical problem is addressed in Orduña and Lourenço (2005).

$$\vec{N}_0\delta\vec{\lambda} - \vec{C}\delta\vec{u} = \vec{0} \tag{1}$$

$$\vec{F}_{\mathrm{v}}^{\mathrm{T}} \cdot \delta\vec{u} - 1 = 0 \tag{2}$$

$$\vec{F}_{\mathrm{c}} + \alpha\vec{F}_{\mathrm{v}} - \vec{C}^{\mathrm{T}}\vec{Q} = \vec{0} \tag{3}$$

$$\vec{\varphi} \leqslant \vec{0} \tag{4}$$

$$\delta\vec{\lambda} \geqslant \vec{0} \tag{5}$$

$$\vec{\varphi}^{\mathrm{T}} \cdot \delta\vec{\lambda} = 0 \tag{6}$$

This set of equations represents a case known in the mathematical programming literature as a mixed complementarity problem (MCP) (Ferris and Tin-Loi, 2001). In general, there is no unique solution for this problem in the presence of non-associated flow rules. If the load factor is minimised, as proposed by Baggio and Trovalusci (1998), the solution can severely underestimate the ultimate load factor, as it will be shown by the validation examples of the present paper.

3. The load-path following solution procedure

In this section a load-path following procedure is proposed using the available solution tools. This procedure uses the same limited information as classic limit analysis (no stiffness or softening parameters are needed) and, at the same time, provides an insight into the structural behaviour prior to failure. Nevertheless, the most important feature of this procedure is that it provides better solutions, in terms of both failure mechanism and load factor, than the traditional proposal of minimising the load factor.

The first step is to apply the constant loads, thus, the load factor is fixed to a zero value and only the equilibrium and yield conditions are considered. Since there is no unique solution to this problem, an objective function needs to be introduced. Eqs. (7)–(9) constitute the proposed problem for this first step. Here n_{int} is the total number of interfaces in the model; N_k, is the normal force at the interface (positive in tension, thus, taking only negative or zero values); V_{1k} and V_{2k} are shear forces parallel to the local axes x_1 and x_2, respectively; see Fig. 2; M_{1k} and M_{2k} are the bending moments parallel to the same axes; T_k is the torsion moment; l_{1k} and l_{2k} are the mid-sides of the interface. Fig. 2 shows the local axes and the parameters l_{1k} and l_{2k} for a rectangular interface, for general quadrilateral interfaces, l_{1k} and l_{2k} take equivalent values (Orduña and Lourenço, 2005). The aim of the objective function is to obtain a uniform stress distribution on the structure.

$$\text{minimise:} \quad \sum_{k=1}^{n_{\text{int}}} \left(N_k^2 + V_{1k}^2 + V_{2k}^2 + \left(\frac{M_{1k}}{l_{2k}}\right)^2 + \left(\frac{M_{2k}}{l_{1k}}\right)^2 + \left(\frac{T_k^2}{l_{1k} l_{2k}}\right) \right) \tag{7}$$

$$\text{subject to:} \quad \vec{F}_c - \vec{C}^{\mathrm{T}} \vec{Q} = \vec{0} \tag{8}$$

$$\vec{\varphi} \leqslant \vec{0} \tag{9}$$

Once the constant loads have been applied, the next step is to steadily apply increasing variable loads. In order to do this, the effective compressive stress, f_{cef}, at the interfaces is taken as the minimum value needed to carry the constant loads, f_{cmin}, and the complete limit analysis MCP problem, Eqs. (1)–(6), is solved. An approximation to f_{cmin} can be obtained through the hinging yield condition, Eq. (10). Here, $\varphi_{\text{hinge}\,i}$ is the hinging yield function for the i side of the interface; see Fig. 3; c_1, c_2 and c_3 are constants given by Eqs. (11)–(13). In Eqs. (11) and (12), x_1 and x_2 represent the coordinates of the interface vertices with the superscripts representing the vertex number according to Fig. 3 and obeying a cyclic convention such that for

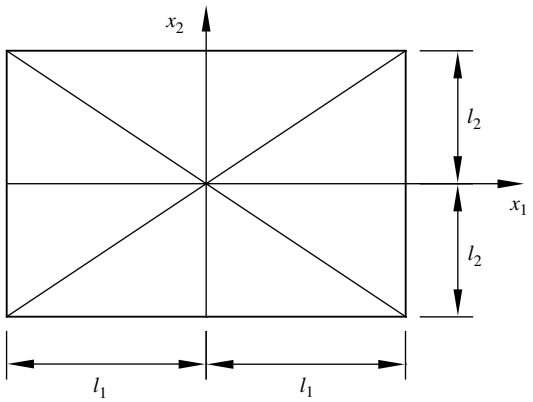

Fig. 2. Rectangular interface.

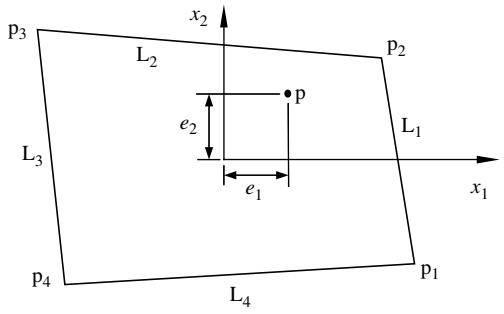

Fig. 3. Interface naming convention.

$i = 4$, then $i + 1 = 1$ holds. In Eq. (13), A_r is the interface area. The expression for f_{cmin} is obtained by solving Eq. (10) with respect to f_{cef}, with $\varphi_{\text{hinge}\,i} = 0$, and adopting the maximum for all interfaces in a structure and for the four hinging modes. So, once obtained the solution for constant loads only, Eq. (14) gives the value of f_{cmin}.

$$\varphi_{\text{hinge}\,i} \equiv c_1^i M_1 + c_2^i M_2 + N + c_3 N^2 \leqslant 0 \tag{10}$$

$$c_1 = \frac{x_1^{i+1} - x_1^i}{x_1^i x_2^{i+1} - x_1^{i+1} x_2^i} \tag{11}$$

$$c_2 = \frac{x_2^{i+1} - x_2^i}{x_1^i x_2^{i+1} - x_1^{i+1} x_2^i} \tag{12}$$

$$c_3 = \frac{1}{A_r f_{\text{cef}}} \tag{13}$$

$$f_{\text{cmin}} = \max_{k=1,n_{\text{int}};\ i=1,4} \left(-\frac{N_k^2}{c_{1k}^i M_{1k} + c_{2k}^i M_{2k} + N_k} \right) \tag{14}$$

The initial guess for this second run is the solution obtained for constant loads only. Applying successive increments to f_{cef}, solutions are computed for the corresponding MCP problems taking as initial guess the solution of the previous step. This process is repeated until reaching the assessed value of the effective stress or until no differences are observed between two successive iterations.

In the load-path following procedure, the normal force at the interfaces is controlled by means of the effective stress. The idea behind this procedure is the fact that the normal force is responsible for providing shear, torsion and bending moment strengths to the interfaces; hence, by controlling the normal forces, the other generalised stresses are indirectly regulated too. Besides, under permanent loads, a relatively uniform stress distribution is expected; later, as the variable loads increase, some parts of the structure crack and slide, while other parts suffer stress concentrations. Cracking, sliding and stress concentrations take eventually the structure to failure upon increasing load. Therefore, by controlling the maximum level of normal stress in the interfaces it is possible to regulate the amount of variable load applied. In this way, by controlling a single parameter, the effective stress, it is possible to take the structure from a state with only permanent loads up to collapse. Conversely, it is necessary to investigate the unloading behaviour of the structure due to the cyclic nature of the variable loads, particularly in the cases of seismic or wind loadings. This is achieved by varying the effective stress from large to small values.

The proposed procedure is summarised here:

(1) Solve the constant loads problem, Eqs. (7)–(9) with $f_{cef} = \infty$.
(2) *Increasing* f_{cef}. Calculate f_{cmin} by using Eq. (14). Make $f_0 = f_{cmin}$. Establish the maximum effective stress f_{cmax} to stop the calculations and perform the following loop:
For $i = 1, 2, \ldots$
$f_i = \zeta f_{i-1}$
solve Eqs. (1)–(6) with $f_{cef} = f_i$
if $f_i \geqslant f_{cmax}$, stop
(3) *Decreasing* f_{cef}. Make $f_0 = f_{cmax}$ and perform the following loop:
For $i = 1, 2, \ldots$
$f_i = f_{i-1}/\zeta$
solve Eqs. (1)–(6) with $f_{cef} = f_i$
if $f_i \leqslant f_{cmin}$, stop

Here ζ is a factor to exponentially increase or decrease the effective stress for successive calculations. This parameter must be larger than one, and recommended values, according to the authors experience, are $1.1 \leqslant \zeta \leqslant 1.4$. The examples shown in this paper were solved by means of a programme made using the GAMS modelling environment (Brooke et al., 1998).

In order to illustrate the application and the kind of results obtained by the load-path following procedure, a two-dimensional model is presented. The two-dimensional limit analysis approach was presented in Orduña and Lourenço (2003) and the model is the *SW30* shear wall presented in that paper. The wall corresponds to a series of tests performed by Oliveira (2003) on shear walls made of dry jointed, stone block masonry under different levels of vertical load and monotonically increasing lateral load; Fig. 4(a). The wall size was 1000×1000 mm, with a thickness of 200 mm. The mean compressive strength, measured on prisms of three and four dry laid stone blocks, was 57.1 N/mm^2. The corresponding effective compressive stress calculated according to Eqs. (15) and (16) is 23.7 N/mm^2. These expressions have been borrowed from reinforced concrete limit analysis theory (Nielsen, 1999) and here f_c is the uniaxial compressive strength of the material in N/mm^2 and v_e is the effectiveness factor. The measured friction coefficient value was 0.66 (Oliveira, 2003). The *SW*30 series consisted of two specimens with 30 kN of vertical load. Fig. 4(b) is the graph obtained for this wall with the load-path following procedure. It is observed that the increasing and decreasing f_{cef} procedures lead to the same results, apart of a small difference for low values of f_{cef}, which is of no concern.

$$f_{cef} = v_e f_c \tag{15}$$

$$v_e = 0.7 - \frac{f_c}{200} \tag{16}$$

More interesting is to see how the load-path following procedure can resemble the intermediate stages of the structural behaviour. Fig. 5 contains pictures of the *SW30* walls during testing. Fig. 6 shows the minimum (compressive) stress distributions on the incremental deformed mesh of a finite element method (FEM) analysis performed for the same wall (Oliveira, 2003). This analysis was done with the DIANA code (DIANA, 1999) and the material model of Lourenço and Rots (1997). Table 1 presents the mechanical properties used in the analysis, where E and v are the Young's and Poisson moduli, respectively, γ_{vol} is the volumetric weight, k_n and k_s are the normal and tangential stiffness, respectively, μ and ψ are the friction coefficient and dilatancy angle, respectively. The tensile strength and cohesion at the interfaces were assumed equal to zero. Finally, Figs. 7 and 8 present the displacement rates and thrusts at the interfaces for selected stages of the load-path following procedure, using limit analysis (increasing f_{cef}).

In the experimental results, and before the development of the final mechanism, sliding in some bed joints at the upper-left part of the wall is evident through the head joints openings. The same sliding does

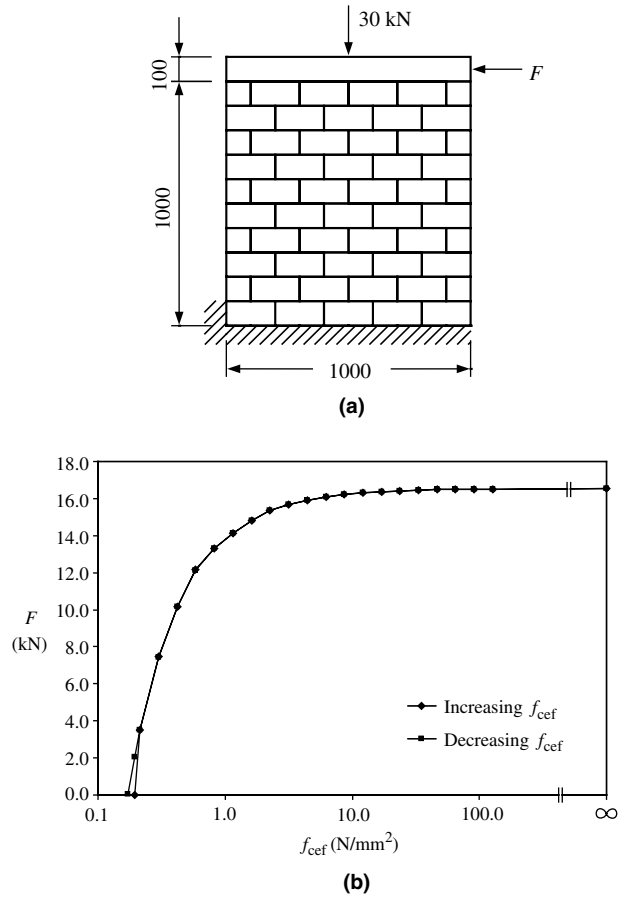

Fig. 4. *SW30* wall: (a) model and (b) load factor vs. effective stress graph.

not appear in the numerical models and is probably caused by the uneven contact at the interfaces in the experimental models due to geometric tolerances in the size of the blocks, which change the process of crack formation significantly.

There is more similitude between FEM and limit analysis results, where perfect initial contact is assumed. In both numerical methods, the wall starts working as a whole. As the horizontal load increases, diagonal stepped cracks form, starting from the lower-right corner and progressing to the wall centre. At the same time, the number of active compressive struts decreases. Finally, the interface stepped crack reaches the central diagonal of the wall, meaning that there is a unique compressive strut, and the wall does not accept more load increments due to the overturning failure mechanism.

Fig. 9 shows the force vs. displacement graphs for the experiments and FEM results (Oliveira, 2003). The calculated limit load appears as a horizontal dotted line. It is noted that the FEM curve approaches asymptotically to the limit analysis load.

Vasconcelos and Lourenço (2004) made cyclic tests on similar walls. Adequate test control and lower tolerances of the size of the units permitted to capture the cracking below the main diagonal at intermediate horizontal loads. These walls were 1.2 m high, 1.0 m wide and 0.2 m thick; Fig. 10(a). The block dimensions were $0.15 \times 0.20 \times 0.20$ m. The measured stone volumetric weight is 25.7 kN/m^3. For analysis purposes, a 0.7 friction coefficient is assumed. Since the stone is of very good quality, the infinite compressive strength

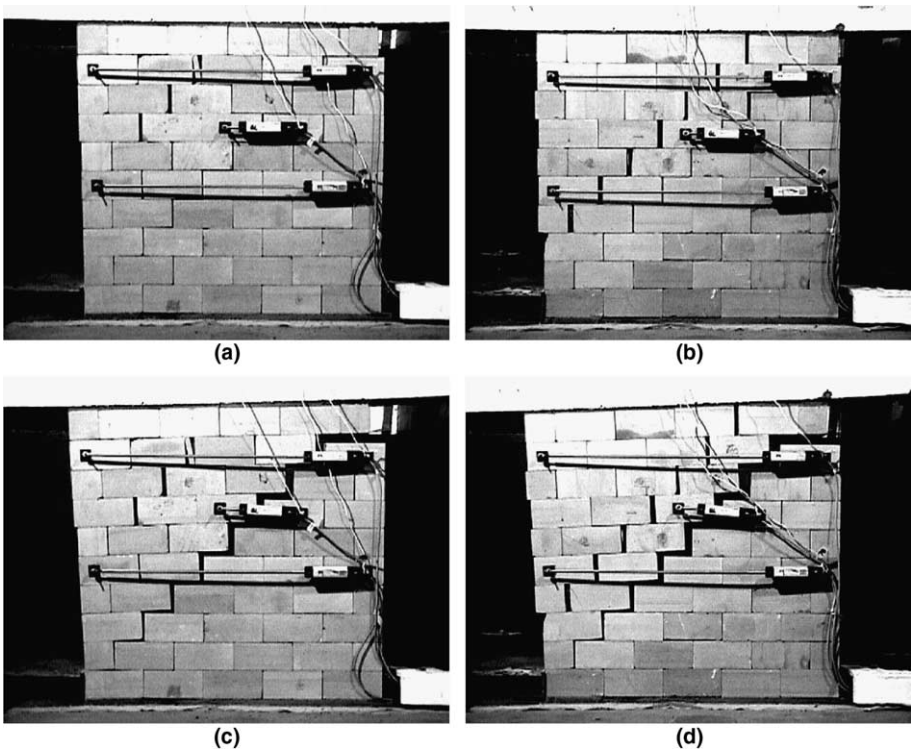

Fig. 5. *SW30* wall during testing; (a–d) crack patterns for increasing horizontal load.

assumption is accepted to approach well the limit state of the wall. A vertical constant load amounting to 250 kN is applied and horizontal, cyclic displacements are imposed through a stiff steel beam. The distance between the specimen's top and the line of horizontal load action is 0.125 m. A total of four specimens with the same characteristics were tested.

Fig. 10(b) shows one of these walls at a moderate displacement state. While Fig. 10(c) presents the displacement rates of the limit analysis model for a moderate effective stress. They do not correspond to the same stage of the structural behaviour, even so, the horizontal forces are similar, but what really matters is that the opened diagonal is the same in both models, i.e. the intermediate behaviour predicted by the numerical model corresponds to a stage of the physical model. Fig. 10(d) and (e) presents the test model and the limit analysis displacement rates, respectively, for the maximum load. Again, the opened diagonal is the same. The maximum loads are not as close as could be expected; however, it is worth to mention that the maximum experimental load for the opposite displacement direction was 92.8 kN and that the mean value for the four specimens and two directions is 91.6 kN, values much more similar to that calculated by limit analysis.

4. Validation

The validation of the three-dimensional model was not an easy task due to the lack of experimental or analytical results to compare with. There are many results of masonry panels with out of plane loading, however in these cases the peak loads largely depend on the masonry tensile strength. There are the results

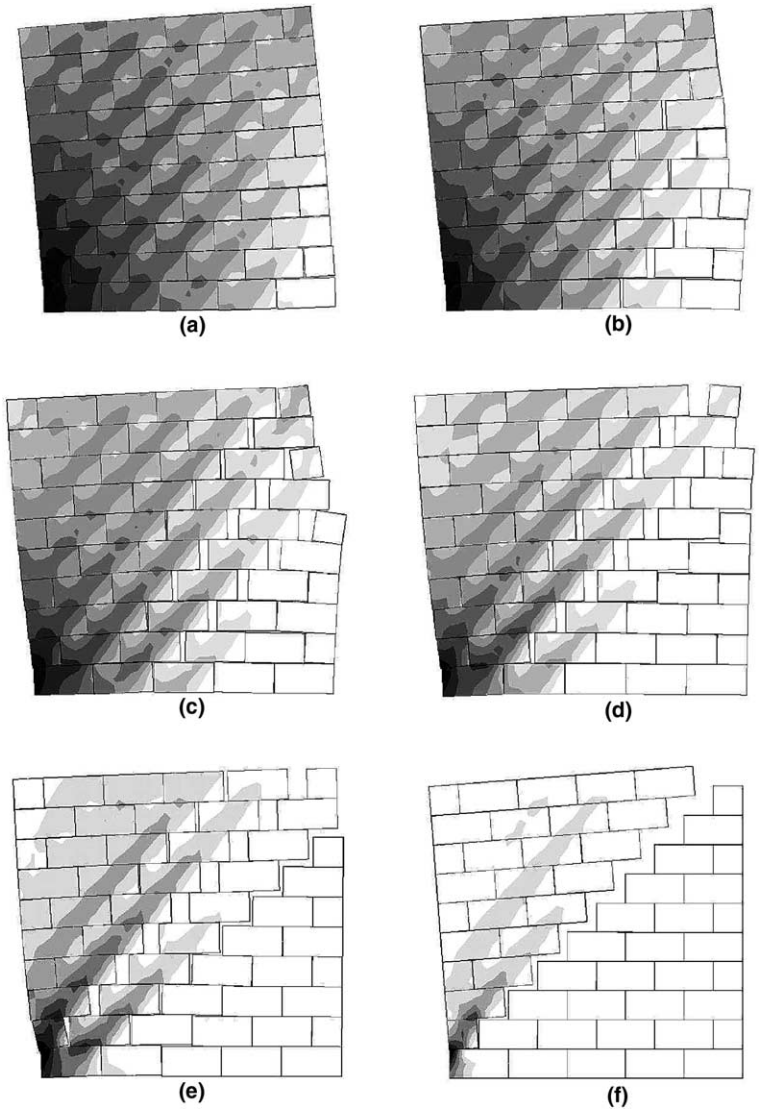

Fig. 6. FEM results for *SW30* wall. Principal compressive stresses depicted on the deformed mesh for a horizontal displacement d (mm) equal to (and horizontal force F in kN): (a) 0.5 (6.0); (b) 1.0 (10.1); (c) 1.5 (12.1); (d) 2.0 (13.3); (e) 3.0 (14.3) and (f) 15.0 (16.3).

Table 1
SW30 wall FEM model mechanical properties

Block			Interface				
E, kN/mm^2	v	γ_{vol}, kN/m^3	k_n, N/mm^3	k_s, N/mm^3	μ	ψ	f_c, N/mm^2
15.5	0.2	25.0	5.87	2.45	0.66	0	57

of Ceradini (1992) on out of plane loaded, dry jointed walls, but these models are too large to be solved by the actually available solution routines. Therefore, the examples presented here are comparisons against

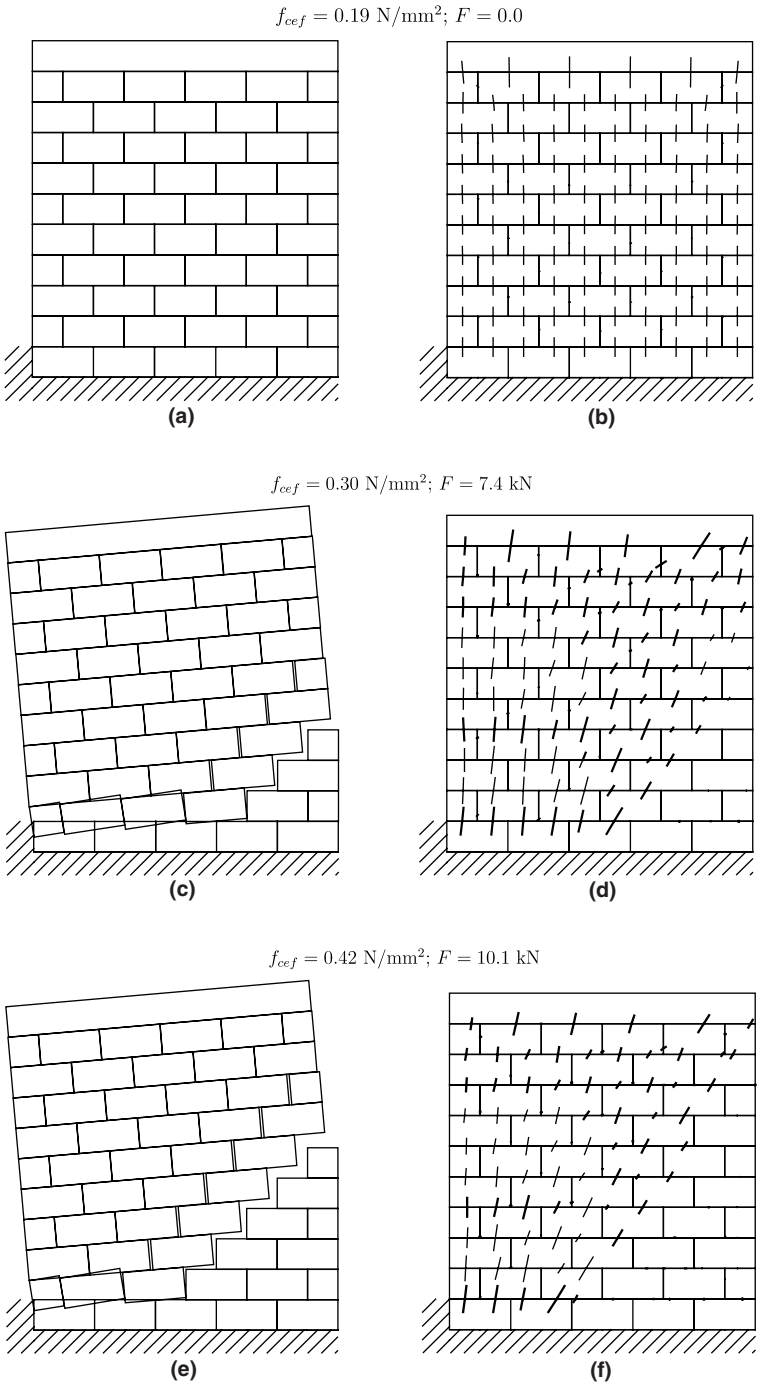

Fig. 7. Limit analysis results for *SW30* wall at different stages; (a,c,e) displacement rates; (b,d,f) thrusts at interfaces.

FEM models. In the three examples presented, comparisons are made against the minimising the load factor procedure in order to show that the load-path following procedure provides better, or at least equally

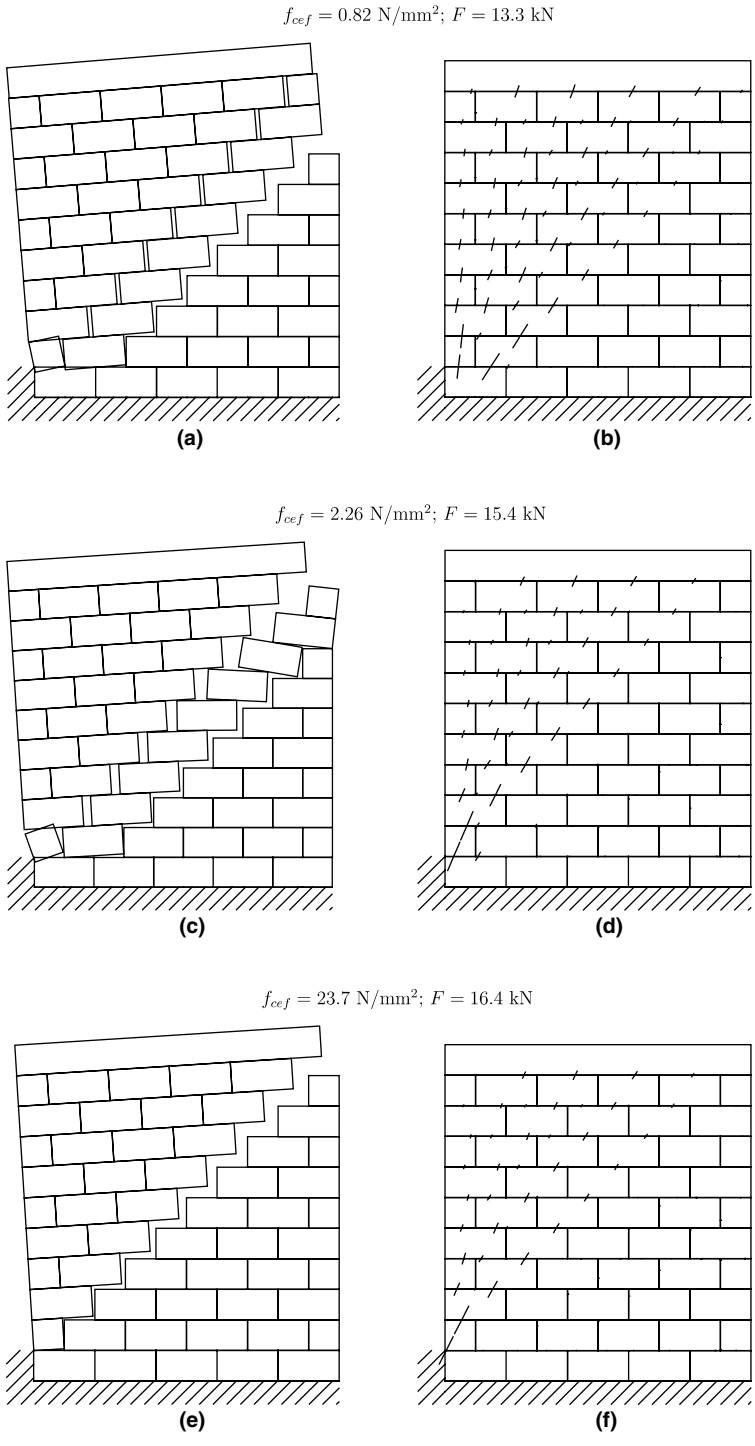

Fig. 8. Limit analysis results for *SW30* wall at different stages (cont.); (a,c,e) displacement rates; (b,d,f) thrusts at interfaces.

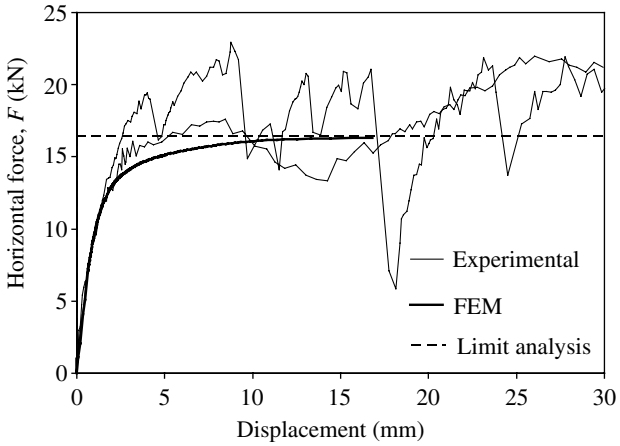

Fig. 9. Horizontal load vs. displacement graph for *SW30* wall.

good solutions than the first one. The selected validation examples are a masonry pile and two walls with out of plane loading.

4.1. Masonry pile

Fig. 11(a) shows the model of a masonry hollow pile. The pile is built of dry masonry blocks with dimensions $0.2 \times 0.2 \times 0.4$ m. The pile dimensions are $0.6 \times 0.8 \times 1.2$ m. The material volumetric weight is 20 kN/m^3 and the friction coefficient is 0.7. The permanent loads are the blocks self-weights. The variable loads are proportional to the blocks weight, but horizontally applied in the direction of the larger base side (X direction). The compressive effective stress, according to the load-path following procedure, is steadily increasing. Also, FEM analyses are performed for different values of compressive strength in order to validate the limit analysis hinging model with limited compressive stress proposed in Orduña and Lourenço (2005). Furthermore, limit analyses, where the load factor is minimised according to the procedure proposed by Ferris and Tin-Loi (2001), are realised in order to compare with the load-path following procedure.

In the FEM model, the blocks were constructed with 20 nodes brick elements joined with 16 nodes interface elements. Table 2 shows the mechanical properties.

Fig. 11 presents also the failure mechanisms obtained for infinite compressive strength. Fig. 11(b) shows the failure mechanism obtained by the FEM analysis. The same failure mechanism is obtained by limit analysis and Fig. 11(c)–(e) shows it from various viewpoints for a better understanding.

A range of ultimate load factors is possible for this mechanism and for infinite compressive strength. It is noted that the ultimate load factor is defined as the ratio between the variable loads causing failure on the structure, and their nominal values, in this case numerically equal to the self-weight of the blocks. Table 3 presents the ultimate load factor obtained from different approaches. If the reaction on the overturning blocks set is concentrated on the *interface A* only, Fig. 11(d), with zero stresses at *interface B*, the ultimate load factor would be 0.427, the minimum possible for this mechanism. If there are non-zero normal and shear contact forces on *interface B*, the last one opposing to the upper block overturning, the maximum possible ultimate load factor for the mechanism shown equals 0.553. The ultimate load factor calculated by minimising the load factor by the procedure proposed by Ferris and Tin-Loi (2001) is 0.427, equal to the minimum possible and 10.8% lower than the factor obtained by FEM. The ultimate load factor calculated with the load-path following procedure is 4.4% higher than the FEM value. In fact the differences in

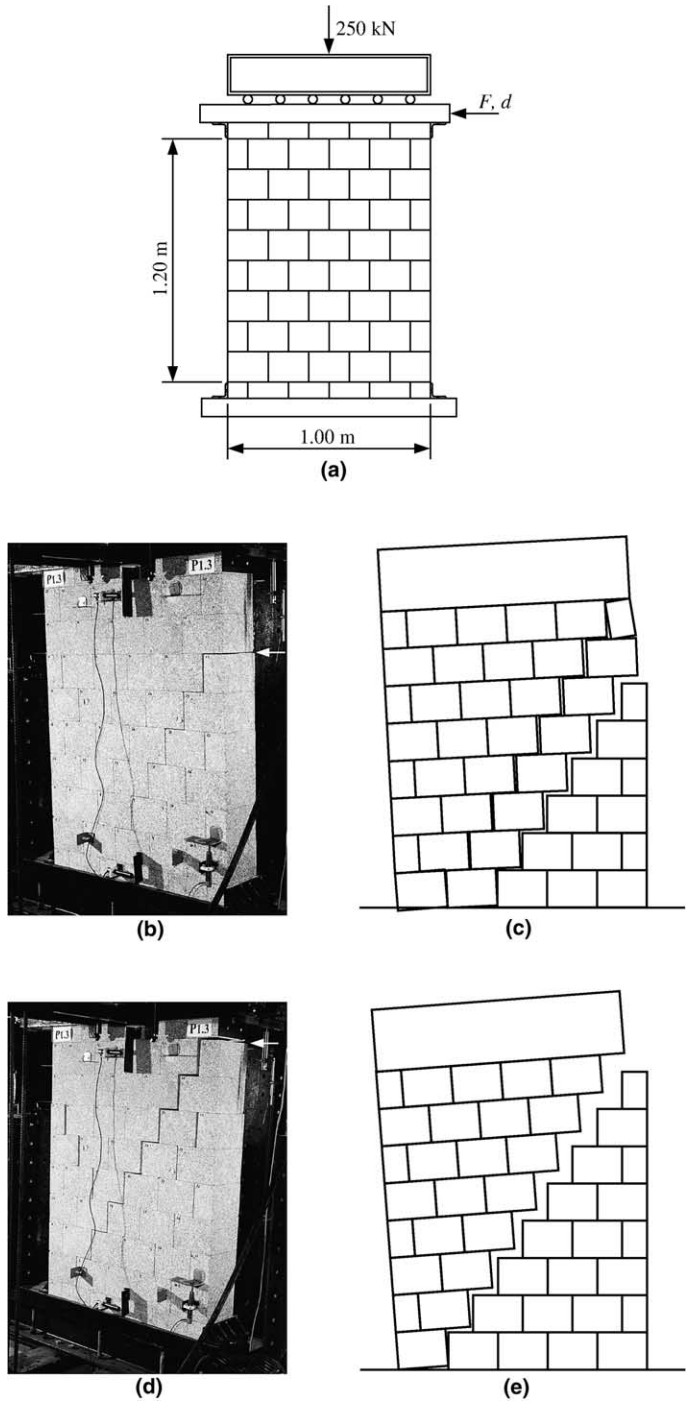

Fig. 10. Vasconcelos shear wall: (a) geometry; (b) test at $d = 11.2$ mm and $F = 81.6$ kN; (c) displacements rates at $f_{cef} = 6.6$ N/mm^2 and $F = 76.1$ kN; (d) test at $d = 23.7$ mm and $F = 86.6$ kN and (e) displacements rates at $f_{cef} = \infty$ and $F = 95.2$ kN.

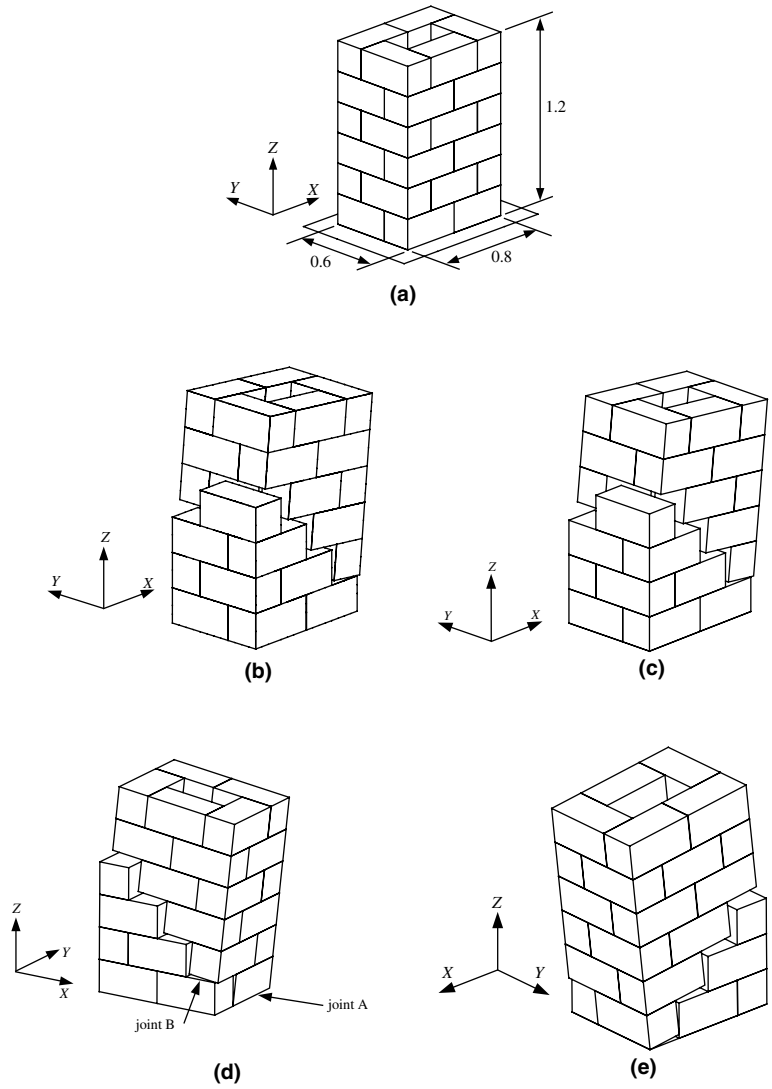

Fig. 11. Masonry pile: (a) model; failure mechanisms for infinite compressive strength; (b) FEM failure mechanism; (c–e) different views of the limit analysis failure mechanism.

Table 2
Mechanical properties for the pile FEM model

Block			Interface				
E, kN/mm^2	v	γ_{vol}, kN/m^3	k_n, N/mm^3	k_s, N/mm^3	μ	ψ	f_c, N/mm^2
1.0	0.2	20.0	2.4×10^3	1.0×10^3	0.7	0	∞

the calculated ultimate load factors are not so large; nevertheless, it is possible to verify that minimising the load factor conducts to lower values than the other procedures and that the load-path following procedure agrees better with the FEM results.

Table 3
Calculated ultimate load factors for infinite compressive strength

Procedure	Ultimate load factor
Theoretically minimum	0.427
Theoretically maximum	0.553
FEM	0.479
Load-path following	0.500
Minimising α	0.427

It is interesting to note that the condition of zero stresses at *interface B* is only possible for an infinite compressive strength. Under limited compressive stresses, the hinge on *interface A* forms slightly inwards and *interface B* must be in contact and must transmit normal and shear forces.

Fig. 12 shows the load factor vs. effective stress graph for this model. Also results for selected values of f_{cef} obtained both by minimising the load factor and by FEM non-linear analysis are represented. It is important to note that the adopted FEM constitutive model in compression is elastic–perfectly plastic in order to agree with the limit analysis hypothesis. It is remembered also, that the aim of this example is not to validate the way in which the effective stress is calculated, but to validate the hinging limit analysis model.

It is observed that minimising α conducts to the same results as the load path following procedure for relatively low values of f_{cef}. Nevertheless, for larger values of f_{cef}, minimising α conducts to decreasing load factors until reaching the minimum possible value for the mechanism shown in Fig. 11. This behaviour is not possible in the load-path following procedure provided that the failure mechanism does not change and the increments in f_{cef} are small, because the mathematical programming routine searches for a solution close to the initial guess given by the previous iteration. Besides, the comparison between the FEM and the load-path following limit analysis results shows good agreement. In particular, the FEM and the load-path following curves show the same trend, without the lowering in the load factor present in the minimising α procedure.

4.2. Masonry walls with out of plane loading

4.2.1. Wall constrained at one edge

Fig. 13(a) presents a wall constrained to horizontal displacements at one edge. The self-weight acts over the wall as constant load, together with variable out of plane forces proportional to the weight.

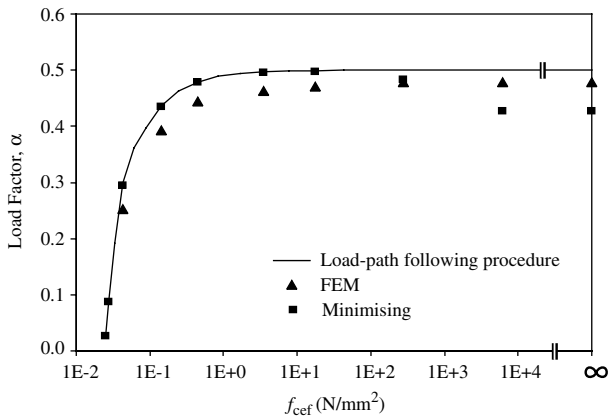

Fig. 12. Masonry pile load factor vs. effective stress graph.

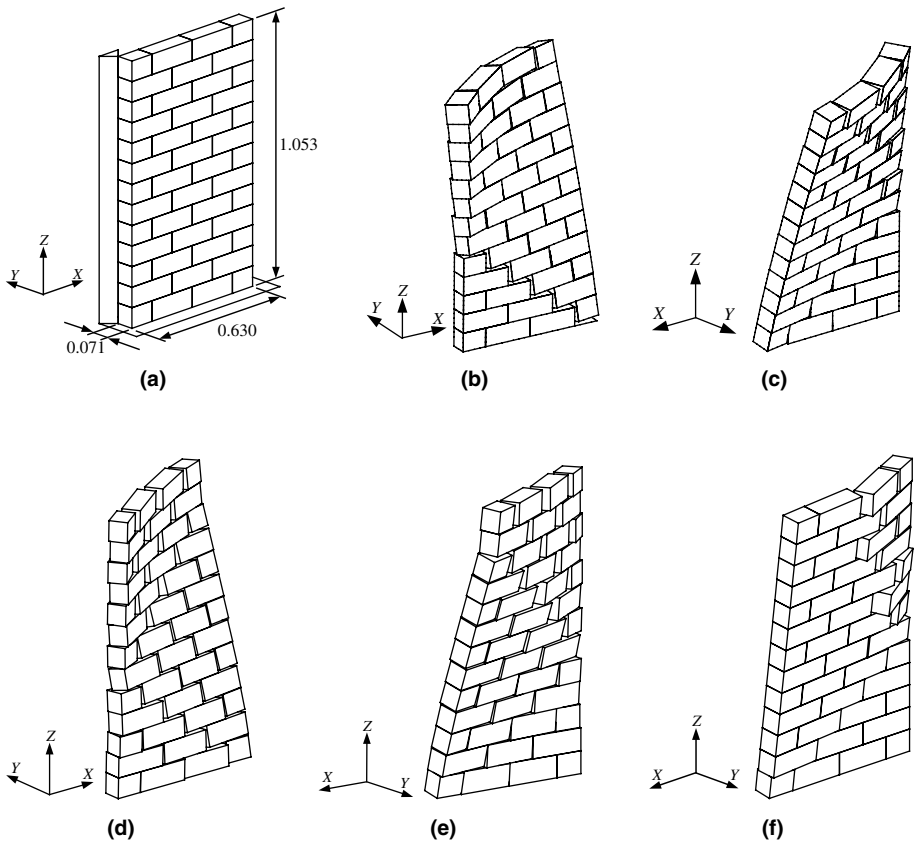

Fig. 13. Out of plane loaded wall, supported at one edge: (a) model; (b,c) FEM failure mechanism for different views ($\alpha = 0.210$); (d,e) limit analysis failure mechanism for different views ($\alpha = 0.216$); and (f) minimising α failure mechanism ($\alpha = 0.127$).

The structure is 1.053 m high, 0.630 m wide and 0.071 m thick, being the block dimensions equal to $0.081 \times 0.210 \times 0.07$ m (height × length × thickness). The volumetric weight is 20 kN/m^3, the friction coefficient is 0.7 and an infinite compressive strength is assumed. The FEM model analysed for comparison purposes has the same element types and elastic properties as in the previous example.

Fig. 13(b)–(c) presents the failure mechanism obtained by FEM for two different views. Fig. 13(d) and (e) shows the limit analysis failure mechanism obtained with the proposed load-path following solution procedure, again for two different views. These mechanisms are not exactly the same; nevertheless, they are similar and it is well known that masonry structures are prone to exhibit slightly different failure modes with minor changes in the collapse load values (Lourenço, 1998). In both mechanisms, two diagonal *yield lines* can be clearly identified: the first going from the bottom of the free edge to the bottom of the sixth row in the constrained edge, and the second one going from here to the bottom of the second row from the top on the free edge. These lines divide the wall into three regions, the lower one does not move at all. The second region rotates over the first yield line and remains almost as a rigid block. And the top region rotates over the second yield line and over the constrained edge, but also presents internal rotations. These internal rotations are evidenced by the different openings of the head interfaces from one side of the wall to the other and are more clearly present in the FEM graph than in the limit analysis one which provides an internal failure more related to sliding. Some of the at sight differences in the failure mechanisms can be also attributed to the different graphical procedures used by the two different post-processors. The FEM output

is produced following the small displacements hypothesis, while the output of the limit analysis results is produced in a large displacements basis. This means that in the FEM output the blocks are deformed but the displacement on each point agrees with the calculations. In the limit analysis output, the blocks preserve their shapes but the displacements are accurate only at the block centroids.

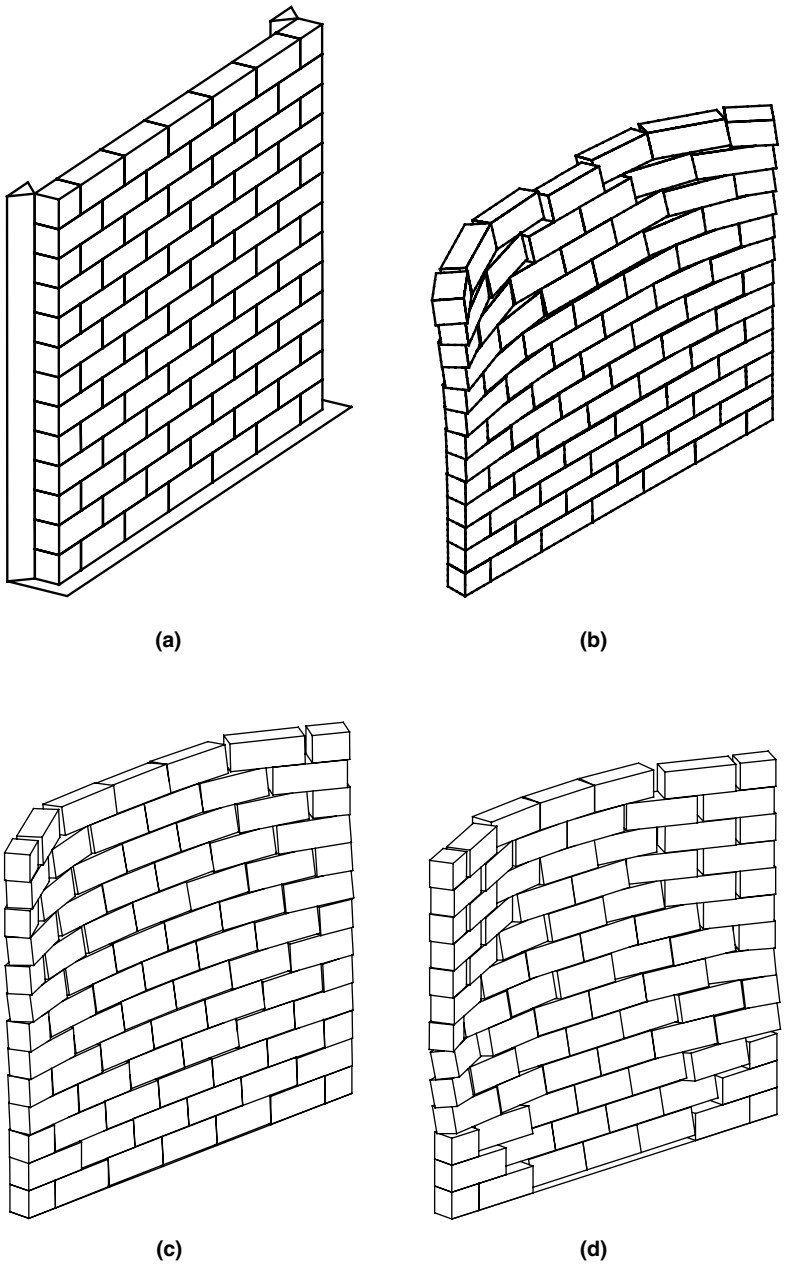

Fig. 14. Out of plane loaded wall, supported at two edges: (a) model; failure mechanisms for (b) FEM analysis ($\alpha = 0.260$); (c) limit analysis ($\alpha = 0.285$) and (d) minimising α limit analysis ($\alpha = 0.193$).

The limit analysis ultimate load factor is similar to the FEM value. This confirms the agreement between the results obtained by the two different methods. Fig. 13(f) presents the failure mechanism obtained minimising the load factor by the procedure proposed by Ferris and Tin-Loi (2001). This mechanism is very different from the previous ones, featuring a general overturning with localised block rotations near the constrained edge. Moreover, the calculated ultimate load factor is unrealistically small, it differs 40% from the FEM value.

4.2.2. Wall constrained at two edges

The wall model presented in Fig. 14(a) has the same properties of the wall in the previous subsection except that it is twice wide, 1.260 m, and it is constrained at both vertical edges. The loading is also composed by the self-weight as constant part and by horizontal, out of plane forces numerically equal to the blocks weights as variable part.

Fig. 14(b)–(d) presents the failure mechanisms obtained by FEM, limit analysis through the proposed load-path following procedure and limit analysis by minimising α, respectively. The former two mechanisms are not equal; nevertheless, they present clear similarities. In both mechanisms, the central part bends around horizontal, longitudinally directed axes with the curvature in the same direction as the variable load, and the external parts, near the supports, bend around vertical axes. These deflections increase from very small at the base to clearly visible magnitudes at the top of the wall. The mechanism resulting from the minimising α procedure is different. In the central part, it has a hinge at the base and the bending curvature around horizontal axes is contrary to the load direction. The mechanism also presents vertical bending near the supports, but with visible magnitude almost from the base until the top of the wall.

The ultimate load factor calculated by the load-path following procedure is 9.5% higher than the resulting from the FEM analysis, which, for engineering purposes, is still an acceptable difference. The ultimate load factor calculated by minimising α is 25.8% lower than the FEM one, and significantly disagrees with the obtained by the other two procedures.

5. Discussion

The results shown in the previous section present two general trends. Firstly, the load-path following procedure always gives slightly larger ultimate load factors than the FEM calculations. This general trend can be attributed to the fact that the piecewise linear yield function used in the limit analysis interface model overestimates the strengths for a number of stress states (Orduña and Lourenço, 2005). Livesley (1992) pointed out the importance of a good interface modelling in the case of three-dimensional limit analysis and, therefore, an improvement of the proposed yield function seems possible. A drawback regarding this issue is the lack of experimental results already mentioned. Nevertheless, the good agreement between limit analysis and FEM results in three different structural models validates also, in an indirect manner, the assumptions made in the yield function development (Orduña and Lourenço, 2005).

The second trend observed in the results of Section 4 is that the ultimate load factor calculated by minimising α is always lower than the one obtained by FEM, reaching this difference 40% in one case. Also, the failure mechanisms obtained by minimising α disagree with those of the FEM, at least in two of three cases, while the load-path following procedure mechanisms are more consistent with the FEM ones. For this reason, it has been stated that the load-path following procedure produces better solutions both in terms of ultimate load factor and failure mechanism than minimising the load factor. Within a direct method theoretical perspective, minimising the load factor seems to be the better and safer choice. Nevertheless, the lack of taking into account the loading history in the limit analysis approach can have a significant impact on the result in the presence of non-associated flow rules. From a practical engineering viewpoint, and considering that the safety assessment is generally based on the maximum reliable strength that a structure can

develop, minimising the load factor can conduct to severe and unacceptable underestimations. The minimising α procedure results shown in Fig. 12 suggest that before to arrive to the last load factor, with infinite effective stress, it is necessary to pass by intermediate mechanisms with larger load factors, in fact similar to that resulting from the load-path following procedure. Therefore, the minimising α results can be regarded, in some cases, as residual strength mechanisms that are generally not useful in the practical assessment of structures.

It is theoretically possible to find all the solutions to the limit analysis MCP, Eqs. (1)–(6), by means of a procedure similar to that proposed by Tin-Loi and Tseng (2003) for linear complementarity problems. Nevertheless, the choice of the most reliable solution must involve the selection of those solutions that are directly reachable from the set of stress states that are possible under gravitational loads only and satisfying the equilibrium and yield conditions, through a continuous stress path with the same requirements, and without having to apply larger load factors than the ultimate load factor. The proposed load-path following procedure is capable of using an initial solution from the set of stress states due to permanent loads only, and take the model until failure due to variable loads. The proposal in this paper is to start from the solution to Eqs. (7)–(9) although, in reality only Eqs. (8) and (9) are necessary. As already stated, Eq. (7) has the objective to obtain an initial uniform stress distribution, but it can be dropped. In the future, it would be of interest to investigate the different solutions that can be obtained, starting from distinct points of the set of gravitational loads only stress states.

6. Conclusions

In the limit analysis theory, the associated flow hypothesis allows for important mathematical simplifications and conducts to three elegant and equivalent formulations, namely the static, kinematic and mixed formulations. Nevertheless, masonry, among other cementitious materials, cannot be properly represented by fully associated flow rules. In particular, the sliding failure mode is non-associated because it features a dilatancy angle significantly lower than the friction angle (the dilatancy angle is taken as zero in this paper). The lack of normality in the flow rules invalidates the simplifications made in classic limit analysis and renders the mixed formulation as the only possibility. Moreover, the presence of non-associated flow rules has a more critical consequence: theoretically, there is no unique solution to the limit analysis problem. The proposal consisting in minimising the load factor can conduct to overconservative results, as shown in this paper. For this reason, a novel load-path following procedure has been proposed. This procedure produces better results and, in addition, provides an insight into the behaviour of structures through the load history until failure with the same limited input data required by standard limit analysis. The procedure has no theoretical foundations at this stage. Nevertheless, this fact does not invalidate the remarkably good results obtained. Many cases exist where an accident or the intuition of the analyst have suggested new procedures and only later a theoretical justifications has been found. The excellent results for masonry structures shown in this paper may be due to the fact that, in the proposed model, the strengths of all failure modes depend on the normal stress. Thus, limiting the amount of normal stress is a natural way to control all the material strengths. The generalisation of this procedure to arbitrary yield functions can constitute a way to solve the non-associated limit analysis problem.

The validation examples have shown that both the limit analysis three-dimensional coupled model presented in Orduña and Lourenço (2005) and the load-path following procedure produce results in agreement with the more precise finite element method. Also, the comparisons of the two-dimensional models against experimental evidence, show that the predicted intermediate and failure behaviours agree well with the observed experimental behaviours. This agreement validates in particular the performance of the load-path following procedure. In three dimensions, comparisons against experimental evidence are desirable; nevertheless, there is a lack of such evidence on dry joints models in the literature. Moreover, it has been found

that experiments on dry joint models are extremely sensible to the initial contact conditions on the joints; therefore, special care must be taken in the geometrical and construction tolerances in the model building process in order to produce results comparable with other methods or experiments.

Acknowledgments

The first author wishes to thank the scholarship made available to pursue his Ph.D. studies by the Consejo Nacional de Ciencia y Tecnología of Mexico. The work was also partially supported by project SAPIENS 33935-99 funded by Fundação para a Ciência e Tecnologia of Portugal.

References

Baggio, C., Trovalusci, P., 1998. Limit analysis for no-tension and frictional three-dimensional discrete systems. Mech. Struct. Mach. 26 (3), 287–304.

Boulbibane, M., Weichert, D., 1997. Application of shakedown theory to soils with non associated flow rules. Mech. Res. Commun. 24 (5), 513–519.

Brooke, A., Kendrick, D., Meeraus, A., Raman, R., Rosenthal, R.E., 1998. GAMS a User's Guide. Tech. rep., GAMS Development Corporation, Washington, DC, USA.

Ceradini, V., 1992. Modelling and experimenting for historic masonry study (in Italian). Ph.D. Thesis. Faculty of Architecture of Rome, La Sapienza.

Corigliano, A., Maier, G., 1995. Dynamic shakedown analysis and bounds for elastoplastic structures with nonassociative, internal variable constitutive laws. Int. J. Solids Struct. 32 (21), 3145–3166.

De Saxcé, G., Bousshine, L., 1998. Limit analysis theorems for implicit standard materials: application to the unilateral contact with dry friction and the non-associated flow rules in soils and rocks. Int. J. Mech. Sci. 40 (4), 387–398.

DIANA, 1999. DIANA User's Manual Release 7.2. TNO Building and Construction Research, Delft, The Netherlands.

Ferris, M., Tin-Loi, F., 2001. Limit analysis of frictional block assemblies as a mathematical program with complementarity constraints. Int. J. Mech. Sci. 43, 209–224.

Livesley, R.K., 1992. A computational model for the limit analysis of three-dimensional masonry structures. Meccanica 27, 161–172.

Lourenço, P.B., 1998. Sensitivity analysis of masonry structures. In: Proc. 8th Canadian Masonry Symp. Jasper, Canada, pp. 563–574.

Lourenço, P., Rots, J., 1997. A multi-surface interface model for the analysis of masonry structures. J. Eng. Mech. 123 (7), 660–668.

Nielsen, M., 1999. Limit Analysis and Concrete Plasticity, second ed. CRC.

Oliveira, D.V., 2003. Experimental and Numerical Analysis of Blocky Masonry Structures under Cyclic Loading. Ph.D. Thesis. University of Minho, Guimarães, Portugal. Available from: <http://www.civil.uminho.pt/masonry>.

Orduña, A., Lourenço, P., 2003. Cap model for limit analysis and strengthening of masonry structures. J. Struct. Eng. 129 (10), 1367–1375.

Orduña, A., Lourenço, P., 2005. Three-dimensional limit analysis of rigid blocks assemblages. Part I: Torsion failure on frictional interfaces and limit analysis formulation. Int. J. Solids Structures, in press, doi:10.1016/j.ijsolstr.2005.02.010.

Palmer, A.C., 1966. A limit theorem for materials with non-associated flow laws. J. de Mécanique 5 (2), 217–222.

Tin-Loi, F., Tseng, P., 2003. Efficient computation of multiple solutions in quasibrittle fracture analysis. Comput. Meth. Appl. Mech. Eng. 192 (11–12), 1377–1388.

Vasconcelos, G. F.M., Lourenço, P.B., 2004. Experimental assessment of the behaviour of unreinforced masonry walls subject to in plane cyclic actions (in Portuguese). In: 6th National Congress on Seismology and Seismic Engineering. Guimarães, Portugal, pp. 531–542.